Bull Earthquake Eng (2010) 8:283–307
DOI 10.1007/s10518-009-9135-4

ORIGINAL RESEARCH PAPER

Analysis of cut-and-cover tunnels against large tectonic deformation

Ioannis Anastasopoulos · George Gazetas

Received: 11 January 2009 / Accepted: 9 April 2009 / Published online: 18 June 2009

Abstract Tunnels are believed to be rather "*insensitive*" to earthquakes. Although a number of case histories seem to favor such an argument, failures and collapses of underground structures in the earthquakes of Kobe (1995), Düzce–Bolu (1999), and Taiwan (1999) have shown that there are exceptions to this "*rule*". Among them: the case of tunnels crossed by fault rupture. This paper presents the analysis and design of two highway cut-and-cover tunnels in Greece against large tectonic dislocation from a normal fault. The analysis, conducted with finite elements, places particular emphasis on realistically modeling the tunnel-soil interface. Soil behavior is modeled thorough an elastoplastic constitutive model with isotropic strain softening, which has been extensively validated through successful predictions of centrifuge model tests. A primary conclusion emerging from the paper is that the design of cut-and-cover structures against large tectonic deformation is quite feasible. It is shown that the rupture path is strongly affected by the presence of the tunnel, leading to development of beneficial stress-relieving phenomena such as diversion, bifurcation, and diffusion. The tunnel may be subjected either to *hogging* deformation when the rupture emerges close to its hanging-wall edge, or to *sagging* deformation when the rupture is near its footwall edge. Paradoxically, the maximum stressing is not always attained with the maximum imposed dislocation. Therefore, the design should be performed on the basis of design envelopes of the internal forces, with respect to the location of the fault rupture *and* the magnitude of dislocation. Although this study was prompted by the needs of a specific project, the method of analysis, the design concepts, and many of the conclusions are sufficiently general to merit wider application.

Keywords Fault rupture · Seismic design · Soil-structure interaction · Cut-and-cover tunnel · Finite element · Constitutive relations · Calibration through experimental data

I. Anastasopoulos · G. Gazetas (✉)
School of Civil Engineering, National Technical University, Athens, Greece
e-mail: gazetas@ath.forthnet.gr

I. Anastasopoulos
e-mail: ianast@civil.ntua.gr

1 Introduction

Tunnels and underground structures have long been considered to suffer little damage in earthquakes and to be safer than above-ground structures (Dowding and Rozen 1978). Several case histories reported in the literature are in favor of such an argument. For example: (a) the Bay Area Rapid Transit (BART) immersed tunnel survived the 1989 Loma Prieta M_s 7.1 earthquake with practically no damage (PB 1991); (b) the Osaka South Port immersed tunnel in Japan also behaved exceptionally during the 1995 M_{JMA} 7.2 Kobe earthquake; (c) a variety of Athens Metro (bored) tunnels and cut-and-cover stations sustained absolutely no damage in the 1999 M_s 5.9 Athens (Greece) earthquake (Gazetas et al. 2005). However, it should be mentioned that all three examples refer to structures that had been indeed designed against seismic loading. The BART tunnel, although built in the 1960s, was one of the first underground structures designed for earthquake loading and equipped with special 3-D joints (Kuesel 1969; Douglas and Warshaw 1971; Bickel and Tanner 1982). The Osaka immersed tunnel, as well as all Athens Metro tunnels, built in the 1990s, had also been designed against earthquake loading according to the latest standards of that time. Moreover, the above tunnels were subjected to substantially smaller seismic intensity levels than their seismic design.

On the other hand, a number of case histories of tunnel damage, or even collapse, are also readily available in the literature. While a systematic review of damage to rock tunnels due to earthquake shaking can be found in Dowding and Rozen (1978), we briefly mention some characteristic examples from recent earthquakes. In the 1995, M_{JMA} 7.2 Kobe earthquake, damage to cut-and-cover box-section reinforced concrete tunnels was quite severe. While the most spectacular failure was the collapse of the Daikai Metro station (Iida et al. 1996; Nakamura et al. 1996), the Yamate line was also heavily damaged (Konagai et al. 2001). Several mountain tunnels in central Taiwan sustained severe damage in the 1999 M_w 7.6 Chi-Chi earthquake. A systematic investigation by Wang et al. (2001) showed that 49 tunnels of 57 (in total) sustained damage from the earthquake. While most of the severely damaged tunnels were on the hanging wall, damage due to dislocation of the seismogenic Chelungpu fault was also reported.

The collapse of a 400 m long section of the under construction 18 m diameter Bolu tunnel in the Düzce (1999) earthquake in Turkey, was arguably affected by the Kaynasli (Düzce–Bolu) fault rupture, although the intensity of shaking has also played a substantial role (O' Rourke et al. 2001).

Several earlier case histories of tunnel damage due to faulting can be found in the literature. One of the earliest such case histories is the failure of the Wrights rail tunnel in the 1906 M_W 7.7 San Francisco earthquake. Built in the 1870s, the tunnel was subjected to an offset of about 1.8 m of the strike-slip San Andreas fault (Prentice and Ponti 1997). Tunnel damage was in the form of cave-ins at the location of fault crossing, accompanied by deformation and cracking over a length of 400 m. It was put back to service about a year later and abandoned in the 1940s. A second well-documented case-history refers to the damage of the Inatori 906 m long tunnel in the 1978 M_{JMA} 7.0 Izu-Oshima-Kinkai (Japan) earthquake: traversed by a strike-slip fault rupture with an offset of about 1 m, it was deformed substantially, requiring substantial repairs (Kawakami 1984).

Admittedly, the relative probability of a structure being damaged from tectonic dislocation is substantially lower compared to shaking. The latter, being the result of waves emitted from the seismogenic fault (due to its "slippage") and propagating over large distances in the earth, affects the ground surface at a much larger area compared to the permanent offset of the fault; the latter is of importance only when the rupture extends to the surface (or near the surface). Even in such a case, the affected area will be an order of magnitude smaller compared to

shaking: a narrow belt along the outcropped rupture, compared to an elliptical "circle" of diameter larger than the length of the fault. Therefore, it is understandable why earthquake engineering research and practice focused in understanding the response of soil-structure systems to ground oscillations, and developing suitable analysis and design methods. Much less effort has been devoted to the response of structures to imposed tectonic dislocation. This lack of insight almost unavoidably lead to over-conservatism: earlier seismic codes had in the past invariably demanded that buildings and important structures not be erected in the immediate vicinity of active faults.

Especially in the case of long structures, such as tunnels and bridges, which cannot easily avoid crossing active fault zones, such a strict prohibition is not only difficult to obey and unduly conservative, but sometimes even meaningless. Because, (a) field evidence from the recent earthquakes in Turkey (Kocaeli and Düzce) and Taiwan (Chi-Chi) has shown that several structures survived large tectonic dislocations almost unscathed (Youd et al. 2000; Erdik 2001; Bray 2001; Ural 2001; Ulusay et al. 2002; Pamuk et al. 2005); (b) earlier studies had also suggested that structures can be designed to withstand large tectonic displacements (Duncan and Lefebvre 1973; Niccum et al. 1976; Youd 1989; Berill 1983); and (c) recent research efforts, combining field studies, centrifuge model testing, and numerical modeling (Anastasopoulos and Gazetas 2007a,b; Bransby et al. 2008a,b; Faccioli et al. 2008; Anastasopoulos et al. 2007, 2008, 2009) have culminated in the development of a validated analysis methodology for the design of structures against surface fault rupture. Moreover, earthquake fault ruptures do not follow precisely the surface of pre-existing faults, but follow planes of weakness within a rather broad shear zone. Thus, attempting to predict the exact location of a fault breakout at the surface is almost meaningless.

The modern trend in some seismic codes is not to prohibit building in the vicinity of active faults, but to demand a case-specific tectonic-geotechnical-structural study to be performed. This paper presents one such case in Greece, dealing with the analysis of two highway cut-and-cover tunnels against large tectonic dislocation.

2 The "Kamena Vourla" bypass and seismotectonics of the area

The under study cut-and-cover tunnels are a part of the "Kamena Vourla" bypass in central Greece, which is one of the key elements of the 550-km highway connecting southern with northern Greece. The typical tunnel cross-section consists of two tubes, 24.4 m in width and 9.5 m in height, and slab and wall thicknesses ranging from 1.0 to 1.4 m (Fig. 1).

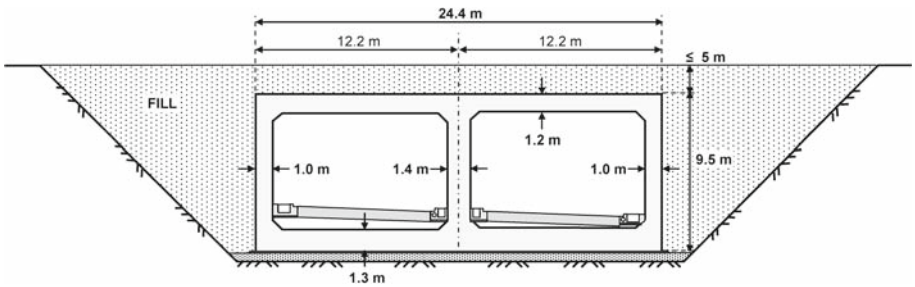

Fig. 1 Typical twin tunnel cross section: geometry and basic dimensions (all dimensions in meters)

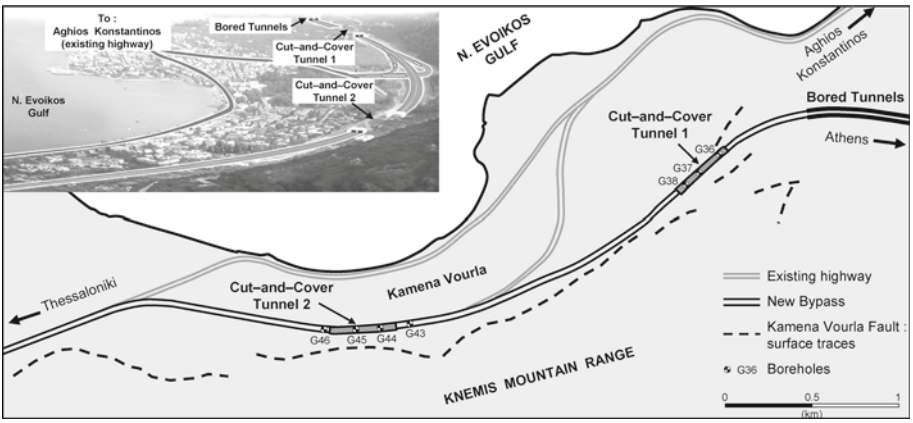

Fig. 2 The Kamena Vourla bypass and the surface trace of the homonymous fault zone

As illustrated in Fig. 2, the alignment of the highway passes through a narrow corridor between the Knemis mountain range and the town of Kamena Vourla, unavoidably crossing the almost in parallel running "Kamena Vourla" fault. The latter is a normal fault of NW–SE direction, forming part of a large fault system, which runs in parallel to the Gulf of Atalanti and the greater Northern Evoikos Gulf, comprising the predominant Atalanti fault, as well as a number of other significant faults (Pantosti et al. 2001).

Being a tectonic graben just to the west of the dextral strike-slip North Anatolian fault zone, the seismic activity of Northern Evoikos is quite intense, characterized by an average horizontal extensional velocity of the order of 5.0 mm/year (Papazachos and Kiratzi 1996). The predominant Atalanti fault was activated in two seismic episodes in 1894: $M \approx 6.5$ and $M \approx 7.0$ (Ambraseys and Jackson 1990; Papazachos and Papazachou 1997). The two earthquakes produced surface fault ruptures of up to 1.5 m and major disturbances of the landscape, over a legth of 40–60 km according to Skouphos (1894), Richter (1958), Rondoyanni (1984), and Pantosti et al. (2001).

Based on this data, in combination with the results of the conducted hazard and seismotectonic studies (OTM 1997), it was decided that the cut-and-cover tunnels (1 and 2, see Fig. 2) be designed to withstand normal tectonic dislocation of vertical offset AD = 1 m ("operating basis" value) and MD = 2 m (maximum possible value).

3 Soil conditions

While the broader area comprises Mesozoic (limestones, sandstones, dolomites and igneous rocks) and Tertiary layers (such as marls, clays, gravels, conglomerates, and marly limestones), the study area is clearly within quaternary sediments: alluvial and lacustrine deposits, and cones of debris.

The geotechnical exploration included SPT measurements and sampling. Its main findings are depicted in Fig. 3. The soil profile consists of alternating layers of silty sand to clayey sand, gravel with cones of debris, and low plasticity clay. Essentially, two soil layers were identified: one consisting of dense silty sand and cones of debris, with number of blows of the standard penetration test, N_{SPT}, in the range of 31–75; the other consisting of very dense silty to clayey gravel, with inter-layers of rock, and with N_{SPT} consistently larger than 50.

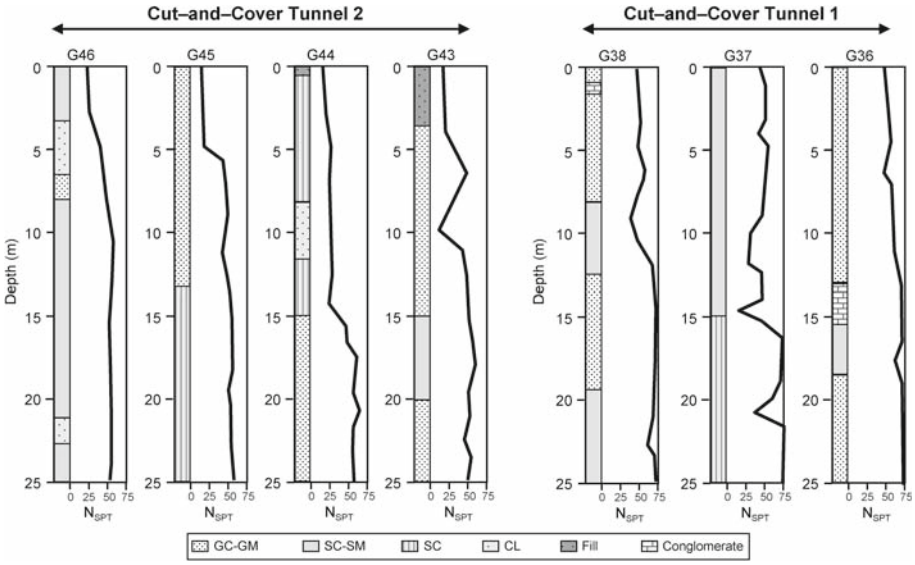

Fig. 3 Compilation of geotechnical data along the axis of the cut-and-cover tunnels: soil characterization and *SPT* blow counts

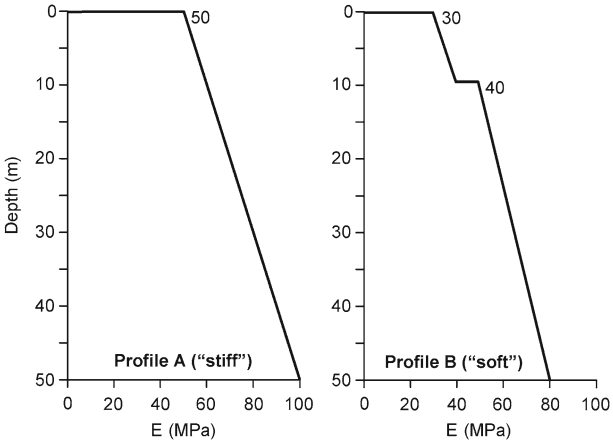

Fig. 4 Idealized soil profiles used for analysis of the cut-and-cover tunnels subjected to tectonic deformation

The first layer is mostly present at the location of Tunnel 2 (top 10 m); the second is mostly present at Tunnel 1.

Thus, in combination with the results of laboratory direct shear and triaxial compression testing, two idealized soil profiles were synthesized (Fig. 4). The first one (soil profile A) is stiffer and mostly relevant to Tunnel 1; the second (soil profile B) is softer and more appropriate for the soil conditions of Tunnel 2.

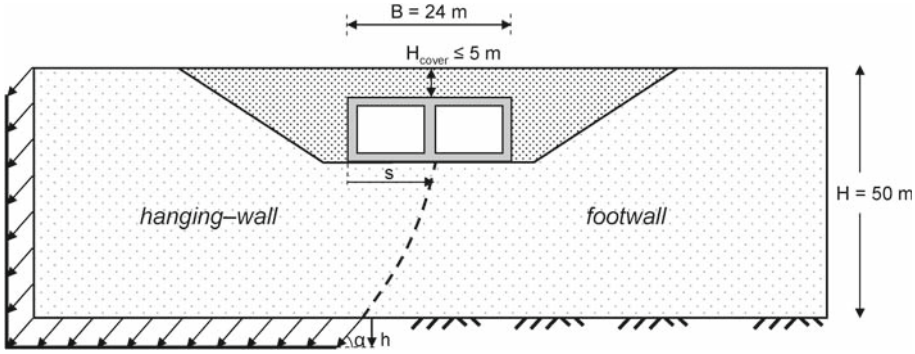

Fig. 5 Problem definition and model dimensions: cut-and-cover tunnel of width $B = 24\,\text{m}$ covered with H_{cover} ranging from 1 to 5 m, subjected to $\alpha = 60°$ normal faulting of maximum vertical offset at bedrock $h = 2\,\text{m}$. The left edge of the tunnel is positioned at distance s from the point where the dislocation would have outcropped in the free field

4 Method of analysis and constitutive modelling

The problem investigated herein is schematically illustrated in Fig. 5. We analyze a soil layer of depth H, at the base of which a normal fault of dip angle α ruptures with offset (downward displacement) of vertical amplitude h. Based on the previously discussed geological and seismotectonic conditions, the depth of the soil deposit is taken equal to $H = 50\,\text{m}$, while $h_{\max} = 2\,\text{m}$ and $\alpha = 60°$.

The analysis is conducted under plane-strain conditions, utilizing the finite element (FE) code ABAQUS. While the soil is modeled with quadrilateral elements, elastic beam elements are used for the tunnel structure ($E = 25\,\text{GPa}$, assuming minor cracking of reinforced concrete). The latter is connected to the soil through special interface elements, allowing for detachment from the bearing soil and relative displacement (sliding). The total width of the model is $B = 4H$, following the (repeatedly validated) earlier recommendation of Bray (1990), Bray et al. (1994a,b) and the quadrilateral elements are $1\,\text{m} \times 1\,\text{m}$ to achieve a reasonably refined mesh [as documented in Anastasopoulos et al. (2007)]. The analysis is performed in two steps. First, fault rupture propagation through soil is analyzed in the free field, ignoring the presence of the tunnel. Then, knowing the location of fault outcropping, the tunnel is positioned so that the unperturbed fault rupture outcrops at distance s from the hanging wall (left) edge of its base slab. With respect to s, three scenarios are investigated: (a) $s = 6\,\text{m}$ (i.e., roughly one fourth of the width from the hanging wall edge of the tunnel); (b) $s = 12\,\text{m}$ (i.e., at the middle); and (c) $s = 18\,\text{m}$ (i.e., about one fourth of the width from the footwall edge). The offset is applied in adequately small consecutive steps.

Soil behavior is modeled with an elastoplastic constitutive model having a Mohr–Coulomb failure criterion and isotropic strain softening, encoded in ABAQUS through a user subroutine (Anastasopoulos et al. 2007). Strain softening is introduced by reducing the mobilised friction angle φ_{mob} and the mobilised dilation angle ψ_{mob} with the increase of plastic octahedral shear strain:

$$\varphi_{\text{mob}} = \begin{cases} \varphi_p - \frac{\varphi_p - \varphi_{\text{res}}}{\gamma_f^P} \gamma_{\text{oct}}^P, & \text{for } 0 \le \gamma_{\text{oct}}^P < \gamma_f^P \\ \varphi_{\text{res}}, & \text{for } \gamma_{\text{oct}}^P \ge \gamma_f^P \end{cases} \tag{1}$$

$$\psi_{\text{mob}} = \left\{ \begin{array}{ll} \psi_p \left(1 - \frac{\gamma_{\text{oct}}^P}{\gamma_f^P}\right), & \text{for } 0 \le \gamma_{\text{oct}}^P < \gamma_f^P \\ \psi_{\text{res}}, & \text{for } \gamma_{\text{oct}}^P \ge \gamma_f^P \end{array} \right\} \tag{2}$$

where: φ_p and φ_{res} the ultimate mobilised friction angle and its residual value; ψ_p the ultimate dilation angle; γ_f^P the plastic octahedral shear strain at the end of softening. Soil behaviour before yielding is modeled as linear elastic, with a secant modulus G_S increasing with depth, in accordance with Fig. 4. Model parameters are calibrated through direct shear test results, and an approximate scaling method is employed to take account of scale effects, as described in more detail in Anastasopoulos et al. (2007). Specifically, the following model parameters were used for the two (already discussed) idealized soil layers:

(a) *Soil layer* 1: $\varphi_p = 35°$, $\varphi_{\text{res}} = 29°$, $\psi_p = 8°$, $\psi_{\text{res}} = 0°$, $c = 5\,\text{kPa}$, and $\nu = 0.30$
(b) *Soil layer* 2: $\varphi_p = 41°$, $\varphi_{\text{res}} = 32°$, $\psi_p = 14°$, $\psi_{\text{res}} = 0°$, $c = 10\,\text{kPa}$, and $\nu = 0.30$

where c is the cohesion and ν the Poisson's ratio. Model parameters for the backfill material (dense sand and gravel), were taken as follows:

Backfill material: $\varphi_p = 46°$, $\varphi_{\text{res}} = 38°$, $\psi_p = 19°$, $\psi_{\text{res}} = 0°$, $c = 2\,\text{kPa}$, and $\nu = 0.30$

In all cases, the selection of model parameters was based on the aforementioned calibration procedure, but with some conservatism and attempting to maintain reasonable consistency with the design recommendations of the geotechnical studies. The friction coefficient at the soil-tunnel interface was assumed equal to 0.8 in all cases.

The modeling methodology employed herein has been extensively validated through: (a) *qualitative* comparisons with the published experimental results of Horsfield (1977) and Cole and Lade (1984), and the case histories of Slemmons (1957), Brune and Allen (1967), and Taylor et al. (1985); (b) *semi-quantitative* comparisons with the observed performance of buildings in Gölcük, Turkey, affected by the Kocaeli 1999 earthquake major fault rupture (Anastasopoulos and Gazetas 2007a,b); and most significantly (c) through *quantitative* blind Class "A" predictions (Lambe 1973) of centrifuge model tests (Anastasopoulos et al. 2007, 2008, 2009).

One such prediction (shown for the first time in this paper) is summarized in Figs. 6 and 7. It refers to a $B = 25\,\text{m}$ rigid foundation with surcharge load $q = 84\,\text{kPa}$, subjected to normal faulting at distance $s = 14.5$ m (notice that the hanging wall is now to the right), through an $H = 25\,\text{m}$ layer of Fontainebleau sand (Gaudin 2002). Model test images and shear strain contours are compared to FE deformed mesh with shear strain contours (Fig. 6). The observed rupture zones (denoted $S1'$ and $S2'$) are compared to the ones that develop in the free-field case ($S1$ and $S2$), i.e., without the presence of the foundation. Initially, for $h \approx 1.23\,\text{m}$, a steep rupture zone $S1'$ propagates half the way to the surface. Compared to $S1$ (i.e., its free-field equivalent), $S1'$ is substantially diverted towards the hanging wall. The analysis does not predict quite such a steep initial rupture zone, but shows a less steep rupture about to emerge beneath the center of the foundation. At the same time, a second rupture starts forming at the footwall (left) edge of the foundation, propagating *from top to bottom*. Although this not particularly clear in the model test image (Fig. 6a), experimental shear strain contours (Fig. 6b) agree fairly well with the numerical prediction. This second rupture starts becoming visible in the centrifuge test image for $h \approx 1.52\,\text{m}$: $S2'$ makes its appearance just to the left of the foundation. It can be seen to correspond to $S2$ of the free-field case, but strongly diverted (by about 10 m) towards the footwall. The numerical prediction ($h = 1.5\,\text{m}$), is quite in line with the experiment. However, while in the centrifuge test shear strain tends to accumulate along $S2'$, the analysis reveals stronger strain localization along $S1'$. Further increase of h to 2.0 m,

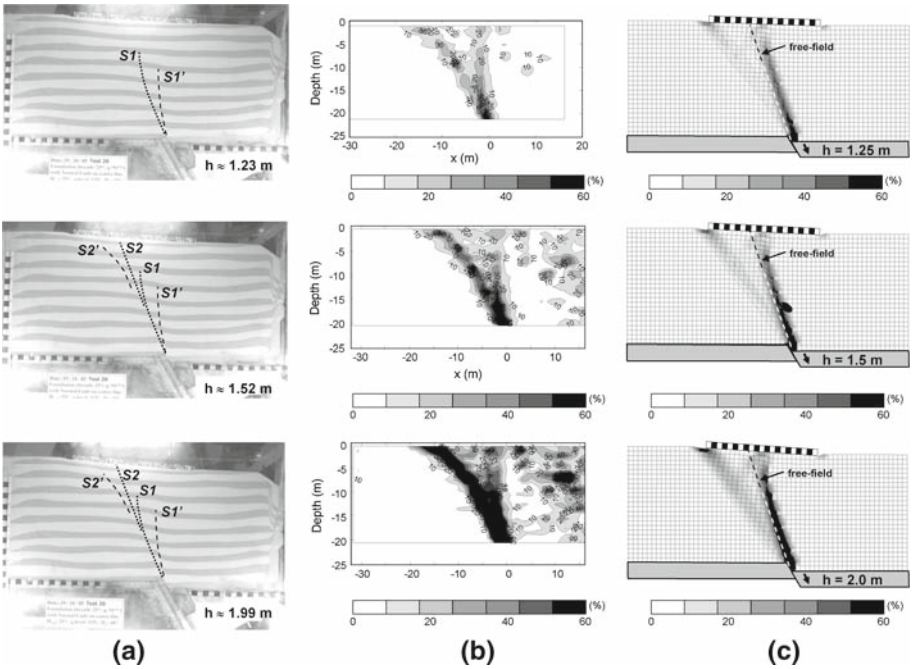

Fig. 6 Class "A" prediction of $B = 25\,\text{m}$ rigid foundation with surcharge load $q = 84\,\text{kPa}$, subjected to normal faulting at distance $s = 14.5\,\text{m}$: **a** centrifuge model test images; **b** experimental shear strain contours; compared to **c** FE predicted deformed mesh with superimposed shear stain contours

leads to deformation localization along $S2'$. Now, analysis and experiment are in very good agreement. The comparison in terms of vertical displacement at the surface is satisfactory for all levels of imposed deformation (Fig. 7).

5 Tunnel response to tectonic dislocation

The results are presented in terms of: (a) deformed mesh with superimposed plastic shear strain contours; (b) tunnel displacement Δ (which is the sum of rigid body motion and structural distortion); (c) structural distortion δ (to better visualize the bending of tunnel slabs and walls); (d) normal contact stresses σ_v and σ_h at tunnel slabs and walls, respectively; and (e) bending moments M of tunnel structural elements. First, we focus on the tunnel with $H_{\text{cover}} = 5\,\text{m}$ in combination with the "soft" soil profile, and elucidate the response of the soil-tunnel system for the three rupturing location scenarios: $s = 6$, 12, and 18 m. We then investigate the role of the overburden pressure (cover) by comparing the response of a tunnel with $H_{\text{cover}} = 1\,\text{m}$. Finally, to unravel the effect of soil compliance we compare the behavior of the tunnel in the "soft" and in the "stiff" soil.

5.1 Tunnel subjected to faulting at $s = 6\,\text{m}$

The response of the tunnel subjected to rupturing close to its hanging wall (left) edge is portrayed in Fig. 8 in terms of deformed mesh with superimposed plastic shear strain contours.

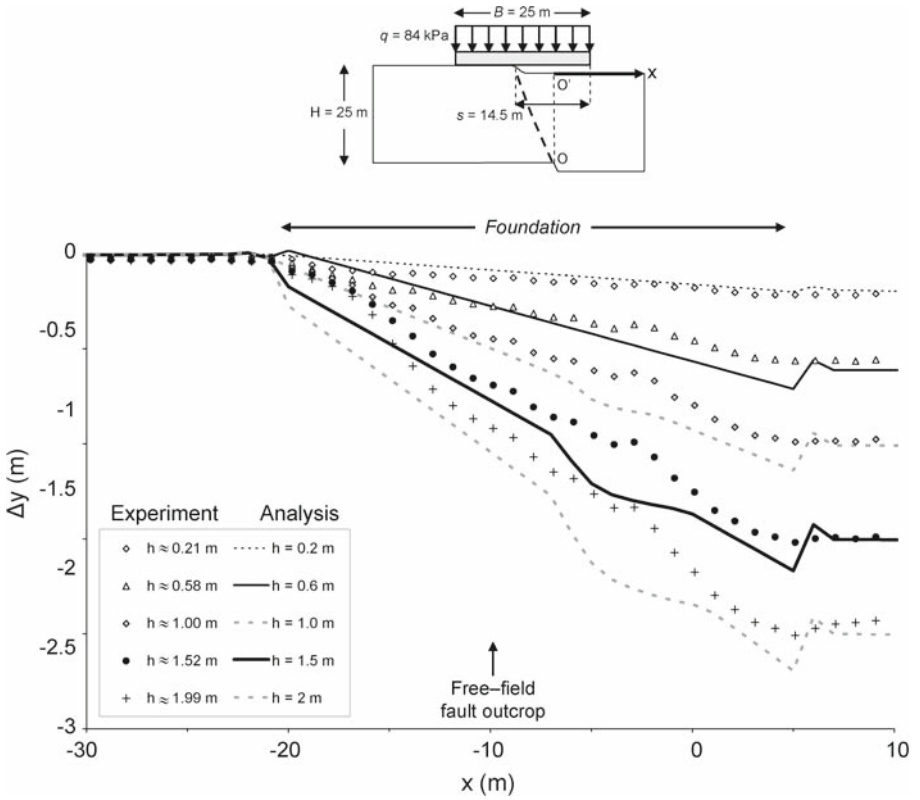

Fig. 7 Class "A" prediction of $B = 25\,\text{m}$ rigid foundation with surcharge load $q = 84\,\text{kPa}$, subjected to normal faulting at distance $s = 14.5\,\text{m}$: comparison of numerical with experimental vertical displacement at the ground surface. Imposed bedrock dislocation $h = 0.4$–$2.5\,\text{m}$

At the beginning, for $h = 0.5\,\text{m}$, a single rupture outcrops close to the left edge of the tunnel. The rupture can be seen to be substantially diverted towards the hanging wall (the dashed line represents the free-field rupture path), without however avoiding the tunnel. Increasing the imposed bedrock displacement to $h = 1.0\,\text{m}$ leads to a pronounced bifurcation of the rupture plane (i.e., a change of mechanism). Now, a second rupture emerges almost at the middle of the bottom slab of the tunnel, while some diffusion can be observed in the same area. At the same time, an *active*-type wedge forms at the left (hanging wall side) of the tunnel, evidently due to the imposed extensional deformation (normal faulting). Further increase of h leads to accumulation of deformation along the already developed rupture planes, and to development of a second also *active*-type wedge at the footwall (right) edge of the tunnel (clearly seen for $h = 2\,\text{m}$).

Figure 9 depicts the evolution of tunnel displacement and distortion with increasing bedrock offset h. The tunnel is subjected to horizontal and vertical displacements, rigid body rotation (Fig. 9a), as well as distortion (Fig. 9b). With the main rupture emerging next to the hanging wall (left) edge of tunnel, the structure is subjected to hogging deformation. Increasing h from 0.5 to 2 m leads to a substantial increase of the rotation of the tunnel. Paradoxically, however, the distortion of some tunnel members tends to decrease with increasing h. To explain it, consider the role of the previously discussed change of mechanism: the bifur-

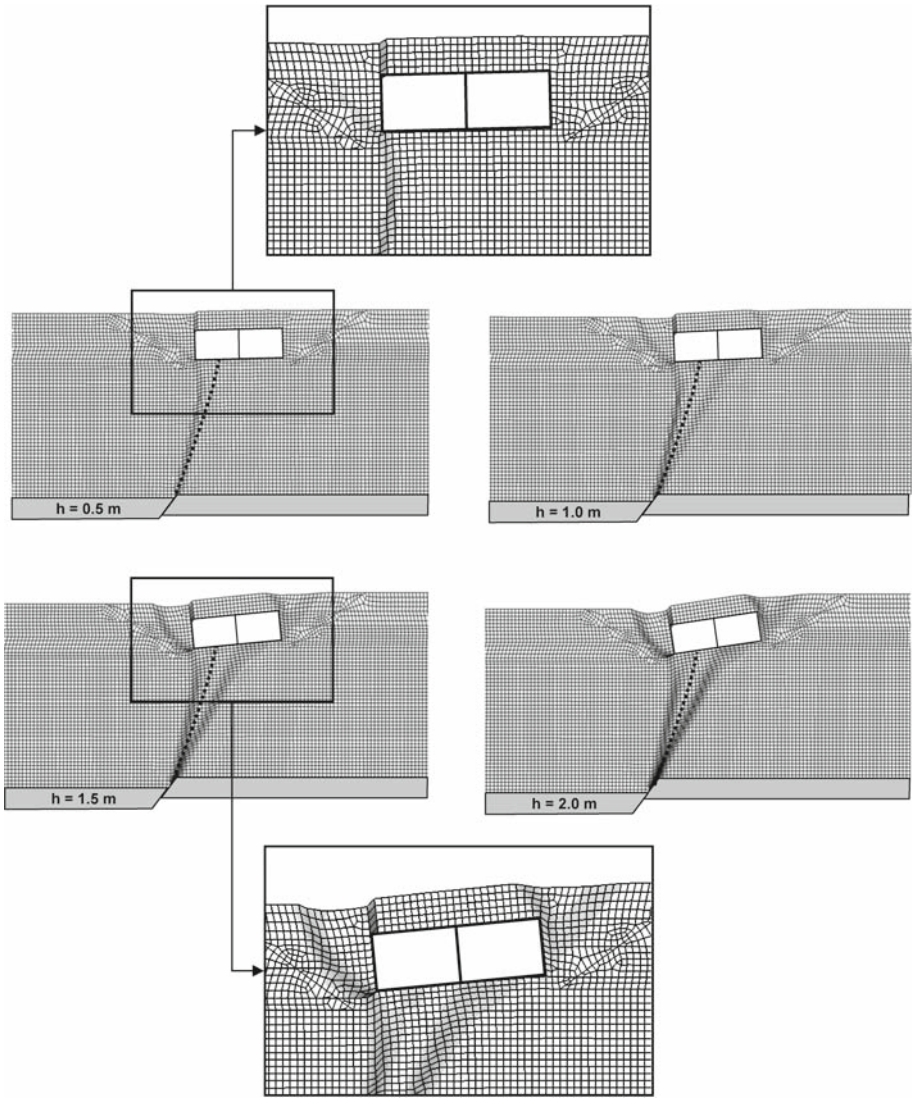

Fig. 8 Tunnel with $H_{\text{cover}} = 5\,\text{m}$ in the "soft" soil profile, subjected to normal faulting at distance $s = 6\,\text{m}$: deformed mesh (deformation scale factor = 2) with superimposed plastic strain contours for bedrock offset $h = 0.5$–$2.0\,\text{m}$ (the *dashed line* represents the free field rupture path)

cation of the rupture plane and the associated diffusion of the tectonic deformation towards the middle of the tunnel seem to act as a stress relief for the tunnel. The effect of this mechanism change is also evident in Fig. 9c: for $h \geq 0.7\,\text{m}$ the slope of Δy (vertical displacement) and Dy (differential displacement, representing the rotation) increases remarkably, while Δx remains almost constant. Evidently, the mechanism change leads to transformation of the imposed deformation to rigid-body rotation rather than structural distortion. Δx is almost insensitive to h: since the tunnel is founded on the footwall, it is not subjected to substantial horizontal displacement.

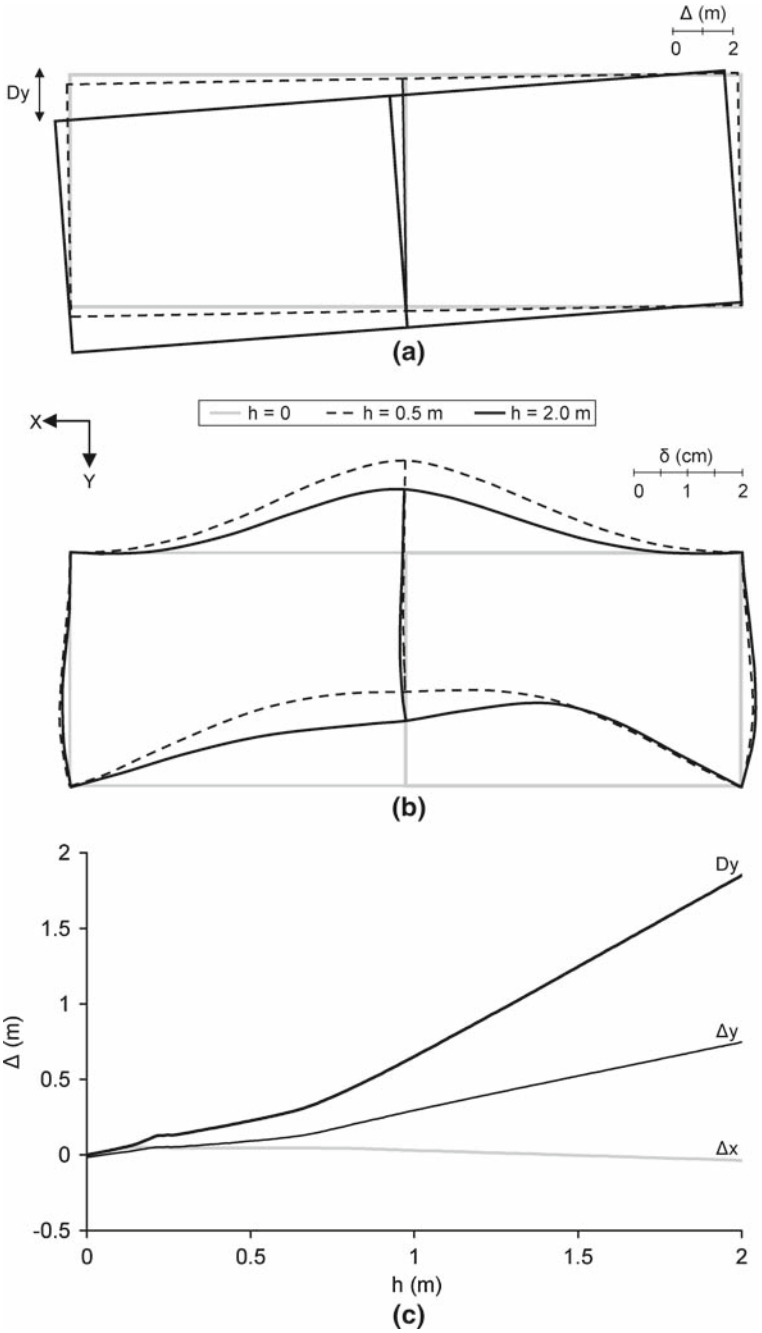

Fig. 9 Tunnel with $H_{\text{cover}} = 5\,\text{m}$ in the "soft" soil profile, subjected to normal faulting at distance $s = 6\,\text{m}$: evolution of **a** tunnel displacement Δ; **b** distortion δ; and **c** horizontal displacement Δx, vertical displacement Δy and differential displacement Dy with the increase of imposed bedrock offset h

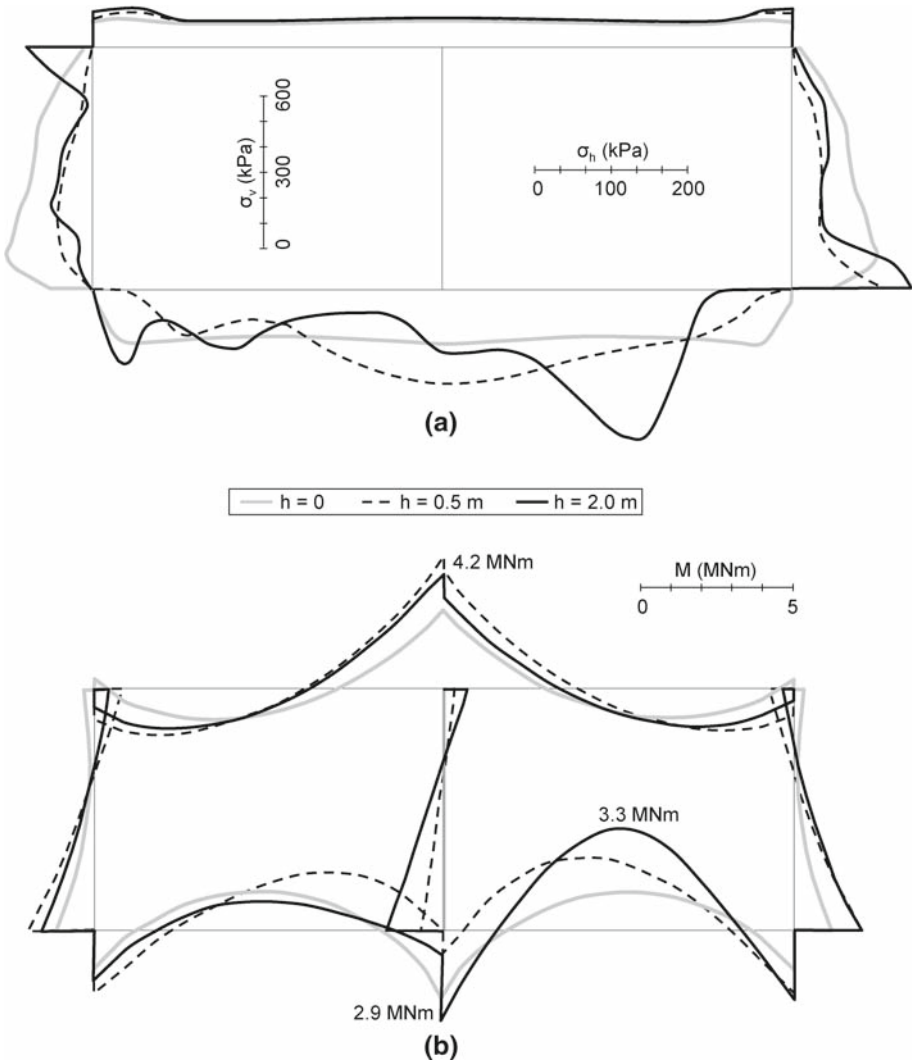

Fig. 10 Tunnel with $H_{\text{cover}} = 5\,\text{m}$ in the "soft" soil profile, subjected to normal faulting at distance $s = 6\,\text{m}$: evolution with increasing imposed bedrock offset h of: **a** tunnel contact stresses σ_v and σ_h: **b** bending moments M

Figure 10 illustrates the contact normal stresses σ_v and σ_h and bending moments M of tunnel structural elements (slabs and walls). As expected, the normal tractions on the top slab are insensitive to the imposed deformation (Fig. 10a): the soil fill (cover) is displaced along with the tunnel. In stark contrast, bottom slab and side walls are subjected to significant stress changes, which result in tunnel distress. Observe that the horizontal stress σ_h acting on the side walls is decreased substantially with the increase of h: this is due to the already discussed (see also Fig. 8) development of active type conditions. Notice, however, that at the top of the left and at the bottom of the right wall σ_h becomes larger than its initial value (before application of the dislocation, $h = 0$). This is attributed to the rotation of the tunnel (see Fig. 9a), which tends to compress the soil in these areas, locally generating larger stresses

(closer to passive conditions). Notice also the substantial increase of σ_v in the middle of the right side of the tunnel when $h = 2$ m: this is because the tunnel is now supported primarily in this location.

At the bottom slab, the increase of h from 0.5 to 2 m leads only to a 30% increase of the maximum observed M; from 2.5 to 3.3 MNm (Fig. 10b). Evidently, the response of the system is highly non-linear, with a substantial part of the ultimate stressing being already attained when $h \approx 0.5$ m: i.e., roughly for the bedrock offset at which the primary rupture emerges underneath the tunnel. As soon as equilibrium is reached, any further imposed deformation does not seem to cause a substantial increase of the stressing (see also Fig. 9). This response is qualitatively similar to that of slab foundations subjected to faulting (Anastasopoulos et al. 2009). Interestingly, the stressing of the top slab may even be reduced with increasing dislocation: increasing h from 0.5 to 2 m reduces M from 4.2 to 3.9 MNm. The same observation also holds for the left wall. The culprit for this highly nonlinear (resembling "softening") behavior is the aforementioned mechanism change, which acts as a means of stress relief at least for some tunnel elements.

5.2 Tunnel subjected to faulting at $s = 12$ m

We now move the unperturbed fault rupture under the middle of the tunnel. As shown in Fig. 11, for $h = 0.5$ m a single rupture is approaching the base of the tunnel, but without ever outcropping. Compared to the free-field path, it is diverted towards the hanging wall (to the left). As for $s = 6$ m (see Fig. 8), the increase of h to 1.0 m leads to bifurcation of the rupture plane. However, due to the different geometry, the second rupture now emerges very close to the footwall (right) edge of the tunnel. Further increase of h leads to accumulation of deformation along the two rupture planes. Interestingly, a second smaller bifurcation can be observed at the tip of the first rupture, just underneath the bottom slab of the tunnel. Overall, the deformation patterns observed for the tunnel are qualitatively very similar to those for the raft foundation of Fig. 6, which is of almost the same width (25 m) but is subjected to lower surcharge load: 84 kPa, compared to the total load of the soil cover (5 m $\times$ 16 kN/m^3 = 80 kPa) plus the self-weight of the tunnel (roughly some additional 85 kPa). The active-type wedges form almost with the same sequence as for $s = 6$ m.

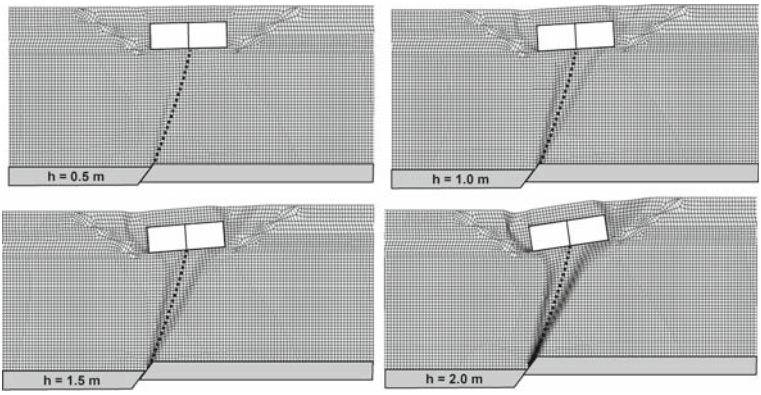

Fig. 11 Tunnel with $H_{\text{cover}} = 5$ in the "soft" soil profile, subjected to normal faulting at distance $s = 12$ m: deformed mesh (deformation scale factor = 2) with superimposed plastic strain contours for bedrock offset $h = 0.5$–2.0 m (the *dashed line* represents the free field rupture path)

The evolution of tunnel displacement and distortion with increasing h is illustrated in Fig. 12. Initially, for $h \leq 0.5$ m, the main rupture approaches the tunnel close to its hanging wall (left) edge, generating *hogging* deformation. However, the increase of the imposed bedrock offset, the bifurcation and the accumulation of additional deformation on the second rupture (which emerges close to the footwall edge) lead to a rather dramatic mechanism change: the structure is now subjected to *sagging* deformation. Again, the response is qualitatively similar to that of raft foundations (Anastasopoulos et al. 2009). In marked contrast to the $s = 6$ m case, the increase of Δy and Dy with h is now almost linear (Fig. 12c). Interestingly, while the maximum Δy (for $h = 2$ m) is larger compared to the previous case (1.15 m instead of 0.75 m for $s = 6$ m), Dy is practically the same (1.85 m, i.e., a 7.6% rotation). Δx is again rather insensitive to h, merely reaching 0.13 m for $h = 2$ m.

Contact stresses σ_v and σ_h, and bending moments M are depicted in Fig. 13. As in the previous case, σ_v at the top slab is insensitive to the imposed deformation (Fig. 13a). Unequivocally, the bottom slab is subjected to substantial stress changes. For $h = 0.5$ m, a rather large stress concentration (increase of σ_v) is observed not far from the middle of the slab, accompanied by decompression at the two edges. In fact, σ_v close to the left edge becomes vanishingly small, indicating that the tunnel almost detaches from the bearing soil. This stress distribution is directly related to the aforementioned hogging deformation of the tunnel. But for $h = 2$ m, the distribution of σ_v changes radically. Stress concentration is now observed at the two edges, with decompression taking place at the middle of the tunnel: *sagging* deformation.

As for $s = 6$ m, the horizontal stresses σ_h acting on the side walls tend to decrease (development of active conditions), with local passive-type stress increases due to tunnel rotation.

The mechanism reversal (from *hogging* to *sagging* deformation) is responsible for the large changes of the bending moment M with increasing h (Fig. 13b). At the bottom slab, with h varying from 0.5 to 2 m a different distribution of M develops: while for $h = 0.5$ m the maximum M takes place at the middle of the right span (2.7 MNm), for $h = 2$ m it is maximized in the middle at the connection with the wall (3.7 MNm). The same observation is valid for the top slab and the side walls: the change of mechanism creates a reversal of the stressing of all tunnel members (with the middle wall being the only exception).

5.3 Tunnel subjected to faulting at $s = 18$ m

Finally, we further move the dislocation close to the footwall (right) edge of the tunnel. Snapshots of deformed mesh with superimposed plastic shear strain contours are shown in Fig. 14. Initially, for $h = 0.5$ m, a single rupture terminates at the base of the tunnel, slightly diverted towards the hanging wall (to the left). As for $s = 12$ m, the increase of h to 1.0 m leads to bifurcation of the rupture plane, with the second rupture now emerging just at the footwall (right) edge of the tunnel. Further increase of h leads to accumulation of most of the additional deformation along the second rupture. As in the previous case, a second smaller bifurcation is observed at the tip of the first rupture. The active-type wedges form again with almost the same sequence, but the one in the footwall side (right) is finally overshadowed by the outcropping rupture plane. At the footwall side wedge, a secondary antithetic rupture and a small gravity graben can be clearly seen for $h \geq 1.5$ m. This extensional feature is largely attributed to the lateral stiffness of the tunnel, which forces the extension to localize in this area.

Figure 15 depicts the evolution of tunnel displacement and distortion with h. Now, the tunnel is always subjected to sagging deformation with the increase of h simply leading to amplified distortion. Again, the response of the tunnel is qualitatively similar to that of

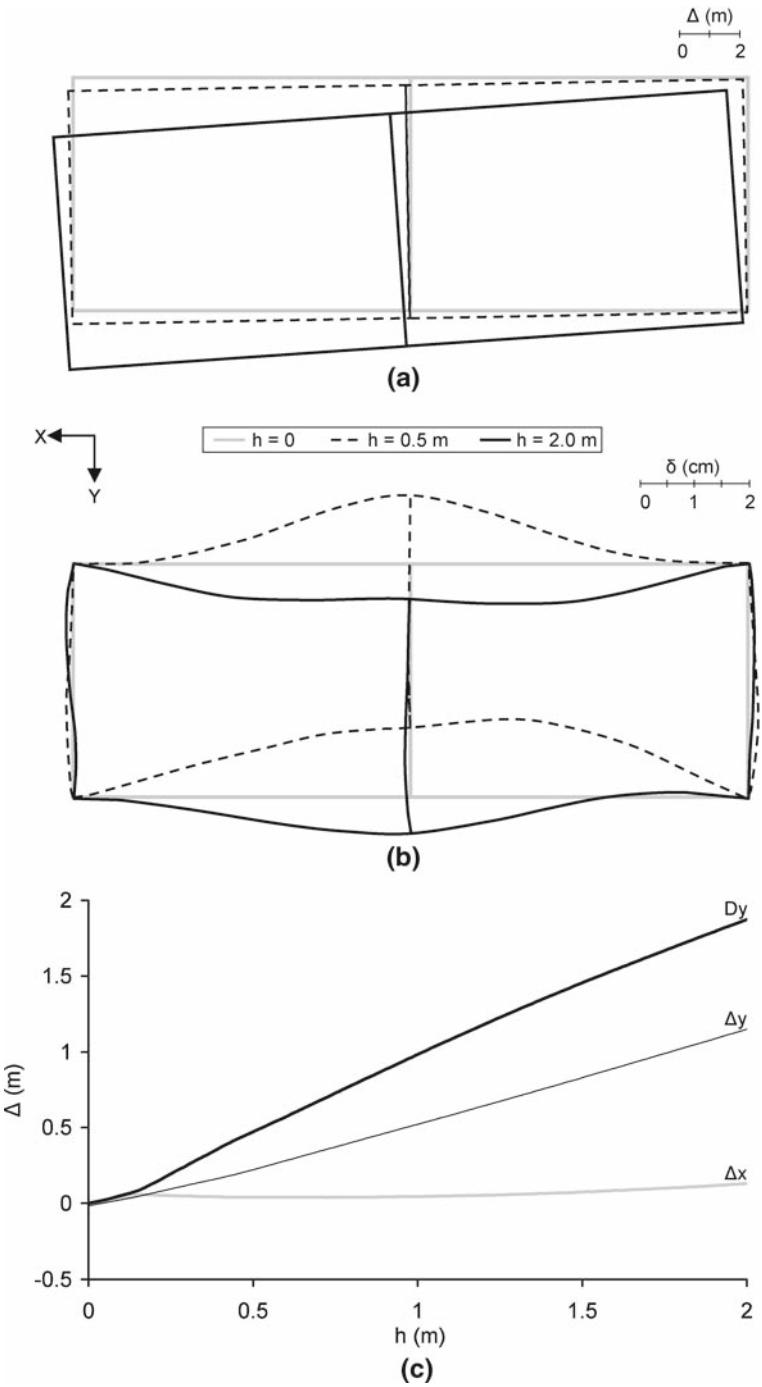

Fig. 12 Tunnel with $H_{\text{cover}} = 5\,\text{m}$ in the "soft" soil profile subjected to normal faulting at distance $s = 12\,\text{m}$: evolution of **a** tunnel displacement Δ; **b** distortion δ; and **c** horizontal displacement Δx vertical displacement Δy and differential displacement Dy with the increase of imposed bedrock offset h

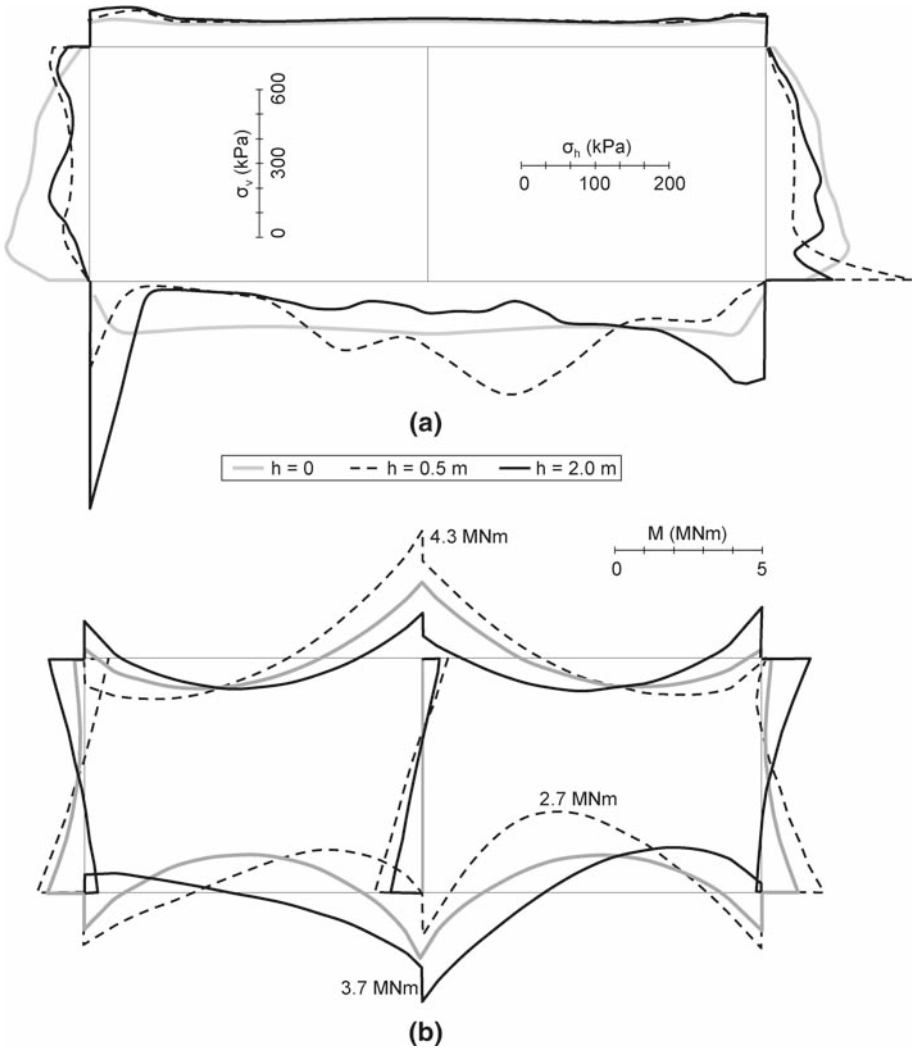

Fig. 13 Tunnel with $H_{\text{cover}} = 5\,\text{m}$ in the "soft" soil profile, subjected to normal faulting at distance $s = 12\,\text{m}$: evolution with increasing imposed bedrock offset h of: **a** tunnel contact stresses σ_v and σ_h; **b** bending moments M

raft foundations (Anastasopoulos et al. 2009). The strong non-linearity of the differential settlement Dy with h in Fig. 15c is attributable to the bifurcation of the initial fault rupture: as soon as the deformation starts accumulating on the second rupture, which outcrops just at the footwall (right) edge of the tunnel, the structure is moving downwards and outwards (to the left) without further increase of its rotation. As a result, while the maximum Dy (for $h = 2\,\text{m}$) is almost one-half of that in the previous cases (0.90 m instead of 1.85 m), Δy is substantially larger (1.58 m instead of 0.75 and 1.15 m for $s = 6$ and 12 m, respectively). Δx is also larger than in the previous cases, reaching 0.64 m (instead of -0.04 and 0.13 m for $s = 6$ and 12 m, respectively).

Figure 16 illustrates the contact stresses (σ_v, σ_h) and bending moments M at tunnel structural elements. In stark contrast with all previous cases, a strong stress increase is now

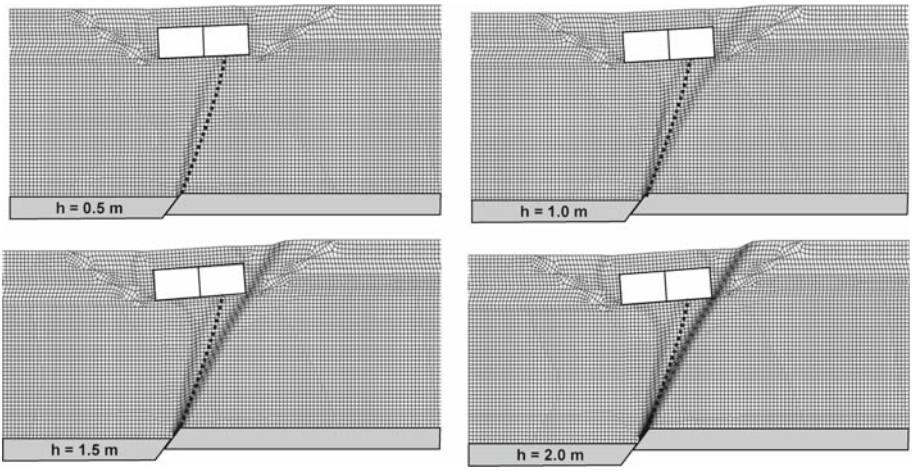

Fig. 14 Tunnel with $H_{\text{cover}} = 5\,\text{m}$ in the "soft" soil profile, subjected to normal faulting at distance $s = 18\,\text{m}$: Deformed mesh (deformation scale factor = 2) with superimposed plastic strain contours for bedrock offset $h = 0.5$–$2.0\,\text{m}$ (the *dashed line* represents the free field rupture path)

observed at the footwall (right) edge of the top slab (Fig. 16b). This is due to the aforementioned formation of a small graben at this area: as the graben tends to move downwards, it finds partial support on the roof slab of the tunnel, thus generating increased σ_v. At the bottom slab, large stresses develop at both edges, with *decompression* and *uplifting* ($\sigma_v \approx 0$) at its middle-left portion. The stress distribution is not altered significantly at larger values of h.

The distribution of horizontal stresses σ_h acting on the left wall (hanging wall side) changes dramatically: form the initial K_o distribution of almost linear increase with depth, to the inverted distribution appropriate for a wall rotating "inwards" about its base. At the top of the wall, passive-type stresses develop due to large tunnel rotation and the presence of overburden pressure. The situation is different for the right wall: while for $h = 0.5\,\text{m}$, σ_h decreases (active type conditions), the ensuing graben formation leads for $h = 2\,\text{m}$ to regaining of the initial (K_o) distribution.

In contrast to what happens for $s = 12\,\text{m}$, the shape of the distribution of M hardly changes with increasing h (Fig. 16b): the tunnel is always subjected to *sagging* deformation. At the right-middle span of the bottom slab, M is largest for $h = 0.5\,\text{m}$ (2.5 MNm); at the connection with the central wall the largest M is attained for $h = 2\,\text{m}$. Notice also that the sagging deformation leads to a substantial reduction of M at the connection of the top slab with the central wall (compared to the $h = 0$ case), and a rather large increase in the connections with the side walls.

5.4 The need for a design envelope

From the previous discussion, it becomes evident that the response of the tunnel depends largely on its location relative to the fault rupture. Unfortunately, however, the exact location of a fault rupture at the ground surface cannot be predicted with accuracy, even if the seismogenic fault is established and "accurately" mapped: the fault trace is neither continuous, nor does it follow precisely pre-existing fault outcrops; the presence of soil deposits further complicates the pattern of fault outcropping. The recent Chi-Chi (1999) earthquake has provided several examples of this unpredictability of the rupture path (e.g., Faccioli et al. 2008).

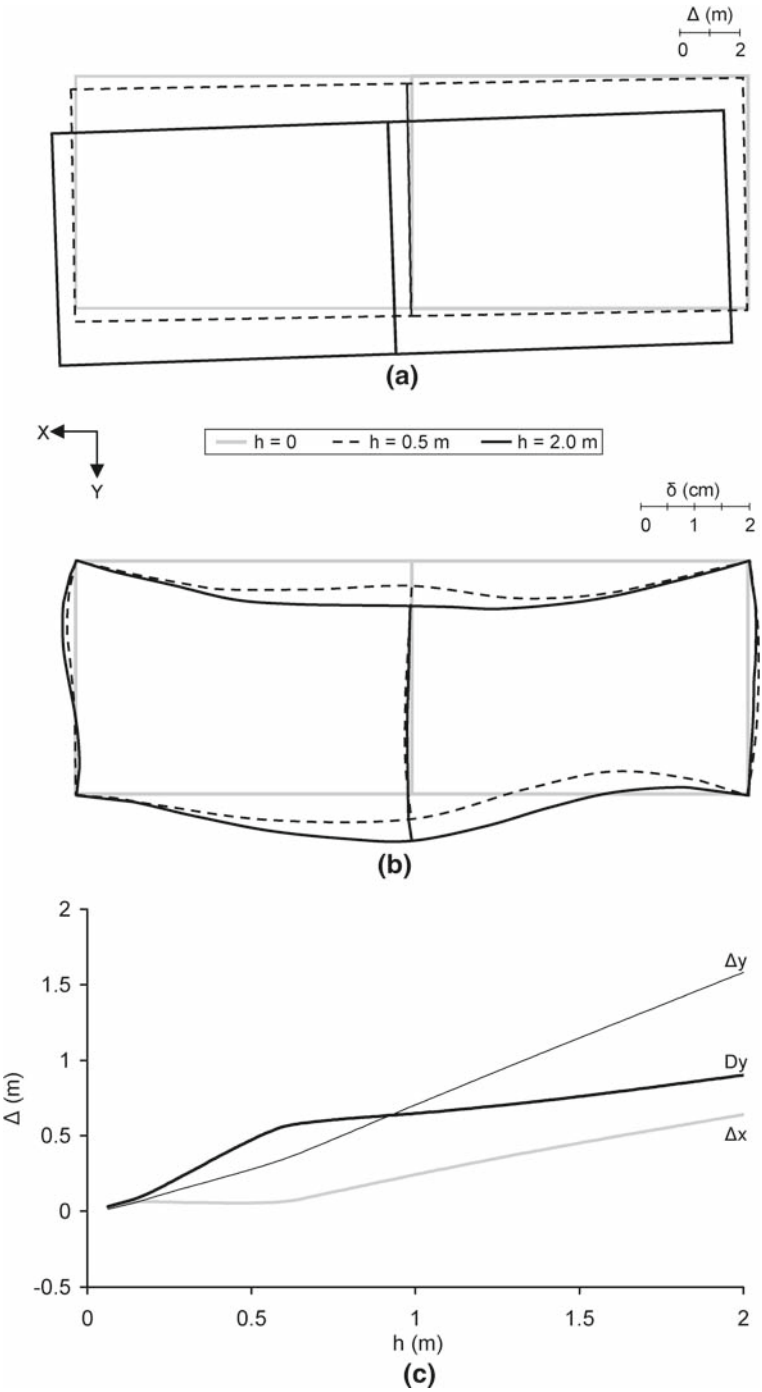

Fig. 15 Tunnel with $H_{\text{cover}} = 5\,\text{m}$ in the "soft" soil profile, subjected to normal faulting at distance $s = 18\,\text{m}$: Evolution of **a** tunnel displacement Δ; **b** distortion δ; and **c** horizontal displacement Δx vertical displacement Δy, and differential displacement Dy with the increase of imposed bedrock offset h

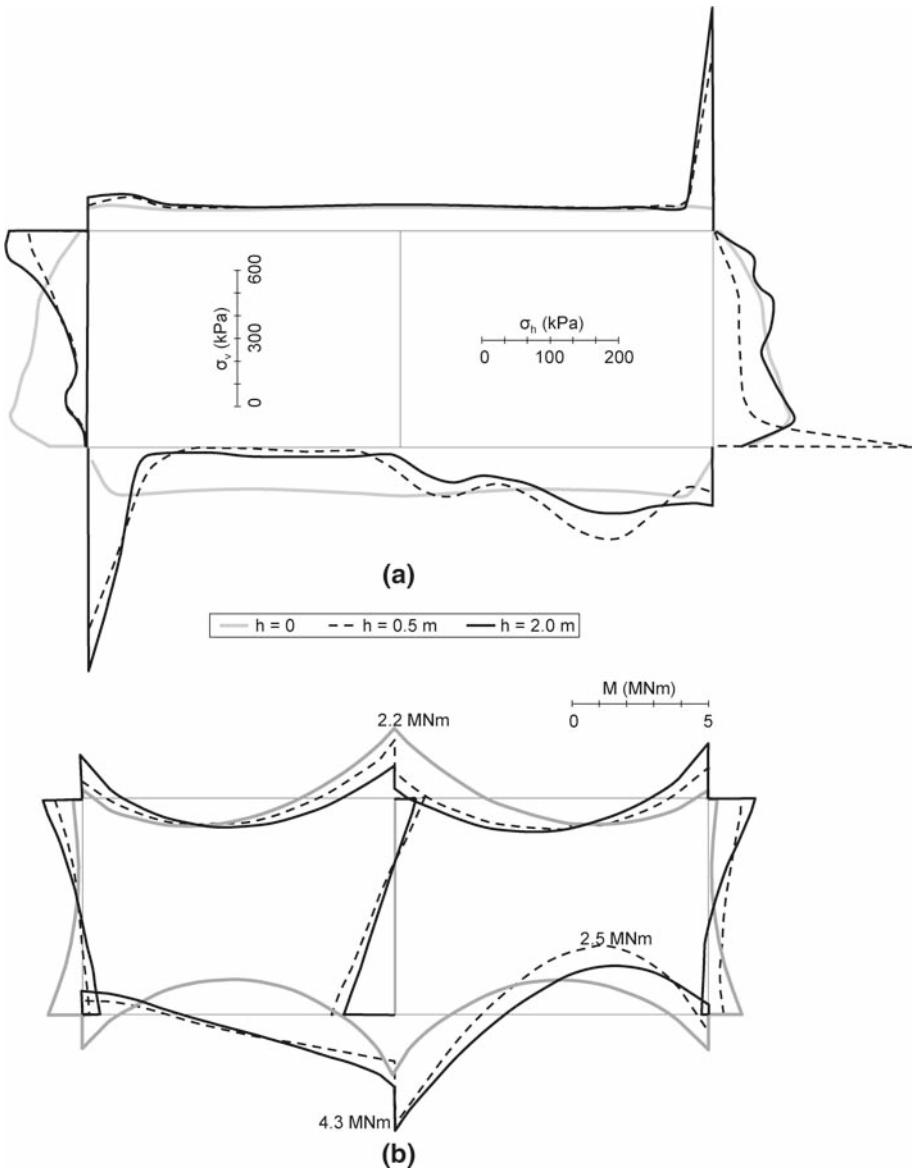

Fig. 16 Tunnel with $H_{\text{cover}} = 5\,\text{m}$ in the "soft" soil profile, subjected to normal faulting at distance $s = 18\,\text{m}$: evolution with increasing imposed bedrock offset h of: **a** tunnel contact stresses σ_v and σ_h; **b** bending moments M

Also, as clearly shown herein, due to the strong non-linearities involved in the interaction of the fault rupture with the tunnel, the maximum stressing is not always attained for the maximum imposed dislocation. Therefore, the design has to be performed on the basis of design envelopes of the internal forces, both with respect to the location of the fault rupture s and the magnitude h of the imposed dislocation (ranging from 0 to its design value). One such bending moment envelope is presented in Fig. 17 for the tunnel with $H_{\text{cover}} = 5\,\text{m}$ on the "soft" soil profile.

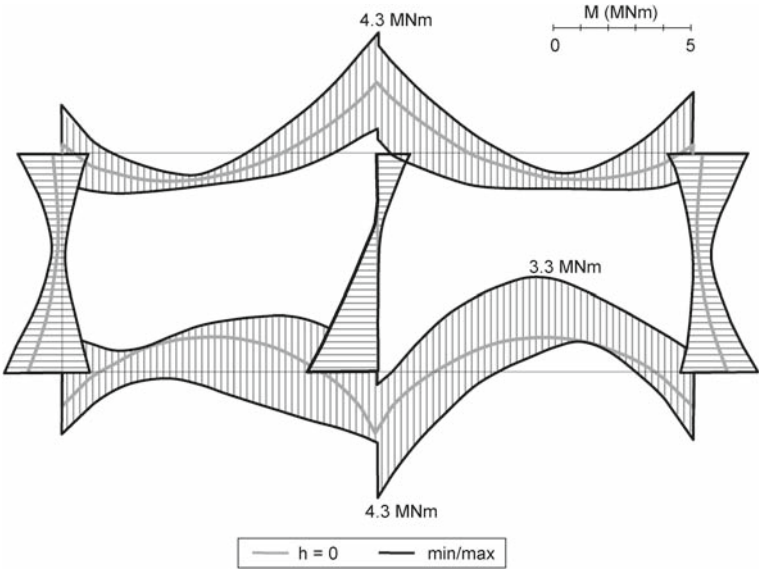

Fig. 17 Tunnel with $H_{\text{cover}} = 5\,\text{m}$ in the "soft" soil profile: bending moment envelopes, for all fault rupture location scenarios and for all levels of imposed bedrock fault offset h

5.5 The effect of the overburden pressure

We compare the response of the tunnel with $H_{\text{cover}} = 5\,\text{m}$ with the case of $H_{\text{cover}} = 1\,\text{m}$, for $s = 6\,\text{m}$. Figure 18a compares the bending moment M of each tunnel for $h = 0$ (i.e., before application of the dislocation) and $h = 2$ m. Evidently, M can be seen to increase substantially with the increase of the surcharge load. However, observe that M for $h = 0$ is also increased with the surcharge load: the stressing of the tunnel is directly related to the pressures transmitted to it by the soil cover. Hence, it is not that rational to compare the stressing of the two tunnels in terms of absolute values of M.

To unravel the real difference in response, in Fig. 18b we present the same comparison but after normalization of M with M_o (the maximum static bending moment for $h = 0$). This normalization with M_o is used as a direct means to show the difference of the tectonically induced distress, compared to the stressing due to the surcharge load due to the soil cover. The differences are now hardly observable, with the heavily loaded tunnel ($H_{\text{cover}} = 5\,\text{m}$) not always suffering the largest distress. As has also been demonstrated in Anastasopoulos et al. (2009) for raft foundations, the role of the surcharge is dual: (a) by pushing the tunnel downwards it compresses the soil underneath, flattening the tectonically-generated "asperities"; (b) it changes the stress field underneath the tunnel, increasing the confining pressures and thereby facilitating stress-relieving phenomena such as diversion, bifurcation, and diffusion.

5.6 The effect of soil compliance

Finally, to demonstrate the effect of soil compliance we compare the response of the tunnel with $H_{\text{cover}} = 3\,\text{m}$ founded in the "soft" or in the "stiff" soil profiles. As shown in the example of Fig. 19 ($s = 6\,\text{m}$), decreasing the soil stiffness is mainly beneficial. An exception is noted at the connection of the bottom slab with the central wall (where the distress of the tunnel in "soft" soil is larger). Other comparisons, not shown herein due to space limitation,

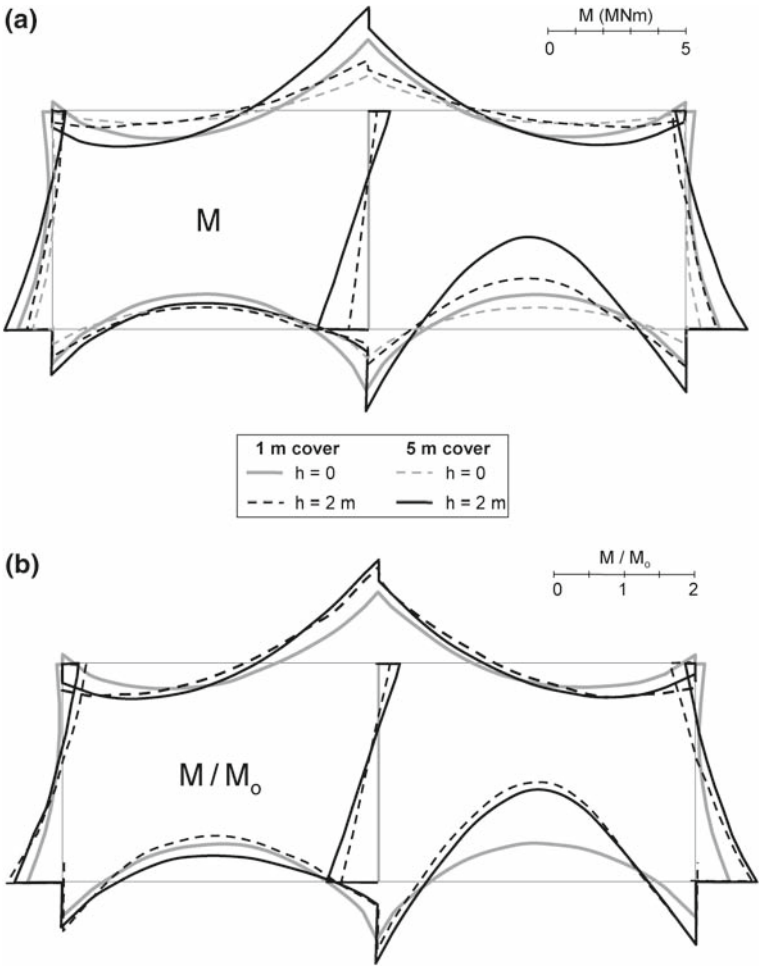

Fig. 18 Illustration of the effect of soil cover: tunnels in the "soft" soil profile, with $H_{\text{cover}} = 1$ or 5 m subjected to $h = 2$ m normal faulting at $s = 6$ m: **a** bending moments M; **b** normalized bending moments M/M_o (M_o: maximum bending moment for $h = 0$ i.e., before application of the tectonic dislocation)

yield the same qualitative result: soil compliance is in general beneficial, at least in terms of stress reduction (the rotation has been found amplified in some soft-soil cases). Although a qualitatively similar conclusion had been drawn from analyses of *buildings* subjected to tectonic dislocation (Anastasopoulos et al. 2008), since there is no certainty that the increase of soil compliance will be beneficial for all elements of a tunnel, a parametric sensitivity analysis is recommended.

6 Conclusions and limitations

This paper has presented the methodology, results, and main conclusions of a special study that was conducted for the design of two highway cut-and-cover tunnels against large tectonic

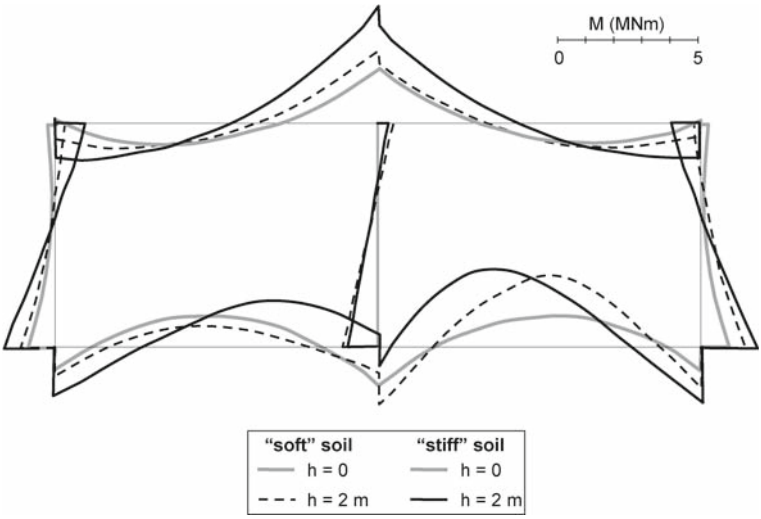

Fig. 19 Illustration of the effect of soil compliance: tunnel with $H_{\text{cover}} = 3\,\text{m}$ in "soft" or "stiff" soil profile, subjected to $h = 2\,\text{m}$ normal faulting at distance $s = 6\,\text{m}$

dislocation. Although the method of analysis employed herein has been extensively validated through successful genuine predictions of centrifuge model tests, there are certain limitations that should be spelled out: (a) Scale effects are taken into account only in an approximate manner; (b) The effect of excess pore water pressures has not been taken into account. If the tunnel is located even partially under the water table, the response may be altered due to different effective stress conditions.

The main conclusions are as follows:

(1) The design of cut-and-cover tunnels against large tectonic dislocation is quite feasible with proper design. Although the study presented in this paper was prompted by the needs of a specific project, the method of analysis, the proposed design concepts, and many of the conclusions presented herein are considered sufficiently general to be applicable in similar projects.
(2) In all cases investigated herein, the rupture path is strongly affected by the presence of the tunnel. The fault rupture is not only diverted, but is also subject to bifurcation and diffusion. More importantly, due to the developing interaction between the tunnel and the rupture, the fault does not outcrop underneath the tunnel in the form of a distinct fault scarp. Instead, the imposed deformation is converted to a diffuse differential displacement acting at the base of the tunnel.
(3) Depending on the position of the tunnel with respect to the emerging fault rupture, the structure may be subjected either to *hogging* deformation (when the rupture outcrops close to its hanging-wall side edge), or to *sagging* deformation (when the rupture is close to its footwall side edge). When the rupture outcrops at the middle, a transition from *hogging* to *sagging* deformation may be observed with increasing dislocation h. Since the exact location of a fault would never be known a-priori, its location relative to the tunnel must be parametrically investigated in design.
(4) Due to strong non-linearities in the soil and the soil-tunnel interface, and the possible mechanism changes associated with the interaction of the fault rupture with the tunnel, the maximum structural stressing is not always attained for the largest imposed disloca-

tion. Therefore, the design has to be performed on the basis of design envelopes of the internal forces, both with respect to the location of the fault rupture, and the magnitude of the imposed dislocation h (ranging from 0 to its design value).

(5) The role of the surcharge load (due to soil cover) is dual: (a) it pushes the tunnel to compress the soil underneath, flattening the faulting-induced anomalies; (b) it increases the confining (normal) stresses underneath the tunnel, facilitating the development of beneficial stress-relieving phenomena such as diversion, bifurcation, and diffusion.

(6) Soil compliance is in general beneficial for the distress of the tunnel, but not necessarily for its rotation. A parametric sensitivity analysis of soil parameters is recommended.

(7) In the specific tunnel examined herein, to safely undertake the stressing of the tunnel due to faulting, the reinforcement ratio had to be increased substantially, but there was no need to increase the thickness of its structural members (slabs and walls). However, it should be mentioned that the dimensioning had already been quite conservative from the beginning, aiming to accommodate large near-fault design accelerations of 0.45 g *and* tectonic deformations.

Acknowledgments This work was partially supported by the Research Program X-SOILS, which was funded by the General Secretariat for Research and Technology of Greece. The authors gratefully acknowledge the structural engineers of the tunnels, Themis Tsimonos and Makis Sykiotis, for their excellent cooperation and thoughtful comments.

References

Ambraseys NN, Jackson JA (1990) Seismicity and associated strain of central Greece between 1890 and 1988. Int J Geophys 126(3):663–708. doi:10.1111/j.1365-246X.1990.tb05577.x

Anastasopoulos I, Gazetas G (2007a) Foundation-structure systems over a rupturing normal fault: part I. Observations after the Kocaeli 1999 earthquake. Bull Earthq Eng 5(3):253–275. doi:10.1007/s10518-007-9029-2

Anastasopoulos I, Gazetas G (2007b) Behaviour of structure-foundation systems over a rupturing normal fault: part II. Analysis of the Kocaeli case histories. Bull Earthq Eng 5(3):277–301. doi:10.1007/s10518-007-9030-9

Anastasopoulos I, Gazetas G, Bransby MF, Davies MCR, El Nahas A (2007) Fault rupture propagation through sand: finite element analysis and validation through centrifuge experiments. J Geotech Geoenviron Eng 133(8):943–958. doi:10.1061/(ASCE)1090-0241(2007)133:8(943)

Anastasopoulos I, Callerio A, Bransby MF, Davies MCR, El Nahas A, Faccioli E, Gazetas G, Masella A, Paolucci R, Pecker A, Rossignol E (2008) Numerical analyses of fault-foundation interaction. Bull Earthq Eng 6(4):645–676. doi:10.1007/s10518-008-9078-1

Anastasopoulos I, Gazetas G, Bransby MF, Davies MCR, El Nahas A (2009) Normal fault rupture interaction with strip foundations. J Geotech Geoenviron Eng 135(3) (in press). doi:10.1061/(ASCE)1090-0241(2009)135:3(359)

Berill JB (1983) Two-dimensional analysis of the effect of fault rupture on buildings with shallow foundations. Soil Dyn Earthq Eng 2(3):156–160. doi:10.1016/0261-7277(83)90012-8

Bickel JO, Tanner DN (1982) Sunken tube tunnels. In: Bickel JO, Keusel TR (eds) Tunnel engineering handbook, Chapter 13. Van Nostrand Reinholds, New York, pp 354–394

Bransby MF, Davies MCR, El Nahas A (2008a) Centrifuge modelling of normal fault-foundation interaction. Bull Earthq Eng 6(4):585–606. doi:10.1007/s10518-008-9079-0

Bransby MF, Davies MCR, El Nahas A (2008b) Centrifuge modelling of reverse fault-foundation interaction. Bull Earthq Eng 6(4):607–628. doi:10.1007/s10518-008-9080-7

Bray JD (1990) The effects of tectonic movements on stresses and deformations in earth embankments. PhD Dissertation, University of California, Berkeley

Bray JD (2001) Developing mitigation measures for the hazards associated with earthquake surface fault rupture. In: Workshop on seismic fault-induced failures—possible remedies for damage to urban facilities. University of Tokyo Press, pp 55–79

Bray JD, Seed RB, Cluff LS, Seed HB (1994a) Earthquake fault rupture propagation through soil. J Geotech Eng 120(3):543–561. doi:10.1061/(ASCE)0733-9410(1994)120:3(543)
Bray JD, Seed RB, Seed HB (1994b) Analysis of earthquake fault rupture propagation through cohesive soil. J Geotech Eng 120(3):562–580. doi:10.1061/(ASCE)0733-9410(1994)120:3(562)
Brune JN, Allen CR (1967) A low-stress-drop, low magnitude earthquake with surface faulting. The Imperial, California, earthquake of March 4, 1966. Bull Seismol Soc Am 57:501–514
Cole DA Jr, Lade PV (1984) Influence zones in alluvium over dip-slip faults. J Geotech Eng 110(5):599–615. doi:10.1061/(ASCE)0733-9410(1984)110:5(599)
Douglas WS, Warshaw R (1971) Design of seismic joint for San Francisco bay tunnel. J Struct Div 97(4):1129–1141
Dowding CH, Rozen A (1978) Damage to rock tunnels from earthquake shaking. J Geotech Eng Div 104(GT2):175–191
Duncan JM, Lefebvre G (1973) Earth pressure on structures due to fault movement. J Soil Mech Found Eng ASCE 99:1153–1163
Erdik M (2001) Report on 1999 Kocaeli and Düzce (Turkey) earthquakes. In: Casciati F, Magonette G (eds) Structural control for civil and infrastructure engineering. World Scientific, London, UK
Faccioli E, Anastasopoulos I, Callerio A, Gazetas G (2008) Case histories of fault-foundation interaction. Bull Earthq Eng 6(4):557–584. doi:10.1007/s10518-008-9089-y
Gazetas G, Gerolymos N, Anastasopoulos I (2005) Response of three Athens metro underground structures in the 1999 Parnitha earthquake. Soil Dyn Earthq Eng 25(7–10):617–633. doi:10.1016/j.soildyn.2004.11.006
Gaudin C (2002) Experimental and theoretical study of the behaviour of supporting walls: validation of design methods. PhD Dissertation, Lab. Cent. des Ponts et Ch., Nantes
Horsfield WT (1977) An experimental approach to basement-controlled faulting. Geologie En Mijnboyw 56(4):363–370
Iida H, Hiroto T, Yoshida N, Iwafuji M (1996) Damage to Daikai subway station. Special issue on geotechnical aspects of the January 17 1995 Hyogoken–Nanbu earthquake. Soils Found 283–300
Kawakami H (1984) Evaluation of deformation of tunnel structure due to Izu-Oshima-Kinkai earthquake of 1978. Earthq Eng Struct Dynam 12:369–383. doi:10.1002/eqe.4290120306
Konagai K, Kamiya H, Nishiyama S (2001) Deformation buildup in soils during the Kobe earthquake of 1995. In: Proceeddings of Workshop on seismic fault induced failures, Tokyo, pp 81–90
Kuesel TR (1969) Earthquake design criteria for subways. J Struct Div ST 6:1213–1231
Lambe TW (1973) Predictions in soil engineering. Geotechnique 23(2):149–202
Nakamura S, Yoshida N, Iwatate T (1996) Damage to Daikai subway station during the 1995 Hyogoken–Nambu earthquake and its investigation. Japan Society of Civil Engineers, Committee of Earthquake Engineering, pp 287–295
Niccum MR, Cluff LS, Chamoro F, Wylie L (1976) Banco Central de Nicaragua: a case history of a high-rise building that survived surface fault rupture. In: Humphrey CB (ed) Engineering geology and soils engineering symposium No. 14. Idaho Transportation Department, Division of Highways, pp 133–144
O' Rourke TD, Goh SH, Menkiti CO, Mair RJ (2001) Highway tunnel performance during the 1999 Düzce earthquake. In: Proceedings of the 15th International Conference on Soil Mechanics and Geotechnical Engineering, August 27–31, Istanbul
OTM (1997) New Athens–Thessaloniki highway, Ag. Konstantinos–Kamena Vourla: seismotectonic study. Technical Report
Pantosti D, De Martini PM, Papanastassiou D, Palyvos N, Lemeille F, Stavrakakis G (2001) A reappraisal of the 1894 Atalanti earthquake surface ruptures, central Greece. Bull Seismol Soc Am 91(4):760–780
Pamuk A, Kalkanb E, Linga HI (2005) Structural and geotechnical impacts of surface rupture on highway structures during recent earthquakes in Turkey. Soil Dyn Earthq Eng 25:581–589
Papazachos CB, Kiratzi AA (1996) A detailed study of the active crustal deformation in the Aegean and surrounding area. Tectonophysics 253(1-2):129–153
Papazachos BC, Papazachou CB (1997) The earthquakes of Greece. P. Ziti Co, Thessaloniki, 304 pp
PB (1991) Trans-bay tube seismic joints post-earthquake evaluation. Parsons, Brinckerhoff, Quade and Douglas Inc., Report prepared for the Bay Area Rapid Transit District
Pecker A guest editor (2008) Integrated approach to fault rupture and soil-foundation interaction. Bull Earthq Eng (Special Issue) 6(4):557–728
Prentice CS, Ponti DJ (1997) Coseismic deformation of the wrights tunnel during the 1906 San Francisco earthquake: a key to understanding 1906 fault slip and 1989 surface ruptures in the southern Santa Cruz Mountains, California. J Geophys Res 102(B1):635–648
Richter CF (1958) Elementary seismology. Freeman, San Francisco, 768 pp

Rondoyanni Th (1984) Etude néotectonique des ravages occidentaux du canal d'Atalanti, Grèce, Centrale. Thèse 3eme cycle, Université de Paris-XI, 190 pp (in French)
Skouphos T (1894) Die zwei grossen Erdbeben in Lokris am 8/20 und 15/27 April 1894 Zeitschrift Ges Erdkunde zu Berlin 24:409–474 (in German)
Slemmons DB (1957) Geological effects of the Dixie Valley-Fairview Peak, Nevada, Earthquakes of December 16, 1954. Bull Seism Soc Am 47(4):353–375
Taylor CL, Cline KM, Page WD, Schwartz DP (1985) The Borah Peak, Idaho earthquake of October 28, 1983—surface faulting and other phenomena. Earthq Spect 2(1):23–49
Ulusay R, Aydan O, Hamada M (2002) The behaviour of structures built on active fault zones: examples from the recent earthquakes of Turkey. Struct Eng Earthq Eng JSCE 19(2):149–167
Ural D (2001) The 1999 Kocaeli and Duzce earthquakes: lessons learned and possible remedies to minimize future Losses. In: Konagai (ed) Proceedings of Workshop on seismic fault induced failures. Tokyo
Wang WL, Wang TT, Su JJ, Lin CH, Seng CR, Huang TH (2001) Assessment of damage in mountain tunnels due to the Taiwan Chi-Chi earthquake. Tunn Undergr Sp Technol 16:133–150
Youd TL (1989) Ground failure damage to buildings during earthquakes. In: Foundation engineering—current principles and practices, vol 1. ASCE, New York, pp 758–770
Youd TL, Bardet J-P, Bray JD (2000) Kocaeli, Turkey, earthquake of August 17, 1999 reconnaissance report. Earthq Spect Suppl A 16:456